SIMULATING SINGLE CRYSTAL COPPER PHOTOCATHODE EMITTANCE*

T. Vecchione#, SLAC National Accelerator Laboratory, Menlo Park, CA 94025, U.S.A.

Abstract

The performance of free-electron lasers depends on the quality of the electron beam used. In some cases this performance can be improved by optimizing the choice of photocathode with respect to emittance. With this in mind, electronic structure calculations have been included in photoemission simulations and used to predict the emittance from single crystal copper photocathodes. The results from different low-index surfaces are reported. Within the model assumptions the Cu(100) surface was identified as having minimal emittance, particularly when illuminated by 266 nm light and extracted in a 60 MV/m gradient. These findings may guide future experimental work, leading to improved machine performance.

INTRODUCTION

In photocathode-based free-electron lasers (FEL) much of the overall emittance comes from the photocathode itself. Surprisingly, the choice of which photocathode to use is often a result of historical precedent rather than systematic study. In these cases it is important to optimize the choice of photocathode with respect to emittance. Reductions in emittance can increase both the brightness and the energy of the x-rays produced and can save money by allowing undulators to be installed that are shorter in length.

Xie published a model that is useful for illustrating the dependence of FEL performance on emittance [1]. In this model the undulator saturation power, P_{sat}, is given as a function of the beam power, P_{beam}

$$P_{sat}[\varepsilon_x] = 1.6\rho[\varepsilon_x]\left(\frac{L_{1d}[\varepsilon_x]}{L_g[\varepsilon_x]}\right)^2 P_{beam} \quad (1)$$

and the saturation length, L_{sat}, is given as a function of the input noise power, P_n.

$$L_{sat}[\varepsilon_x] = L_g[\varepsilon_x] Ln\left[\frac{P_{sat}[\varepsilon_x]}{\alpha P_n}\right] \quad (2)$$

Both the saturation power and the saturation length depend on the FEL parameter, ρ, which in turn depends implicitly on emittance, ε_x, through the beam size, σ_x. The FEL parameter for a planar undulator is given by

$$\rho[\varepsilon_x] = \left(\left(\frac{I}{I_A}\right)\left(\frac{\lambda_u}{2\pi\sigma_x[\varepsilon_x]}\right)^2\left(\frac{1}{2\gamma}\right)^3 \times \left(\frac{K}{\sqrt{2}}\left(J_0\left[\frac{K^2}{4+2K^2}\right]-J_1\left[\frac{K^2}{4+2K^2}\right]\right)\right)^2\right)^{1/3} \quad (3)$$

For the sake of brevity, all other important definitions can be found in either [1] or in a comprehensive review of FEL theory by Huang and Kim [2].

Figure 1 uses Eq. (1), (2) and (3) to plot the projected percent increase in radiated power and the percent decrease in saturation length as functions of a percent decrease in emittance for the LCLS-I.

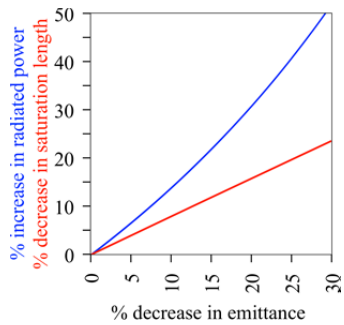

Figure 1: A significant improvement in FEL performance is predicted from lower emittance. For the LCLS-I at 8 keV and an initial emittance of 1 μm a 20% decrease in emittance gives either a 31% increase in radiated power or a 16% decrease in saturation length.

It is reasonable to assume that a change in emittance at the photocathode will lead to a similar change in emittance at the undulator.

The biggest challenge in evaluating photocathodes for use in FELs is in accurately predicting their emittance. Analytical expressions for metal photocathdoes have been derived by Dowell and Schmerge [3], Eq. (4), and by Vecchione [4], Eq. (5). Equation (5) maintains the full Fermi-Dirac distribution in the final result. One consequence of this is that the emittance at non-zero temperatures is non-zero even when the photon energy, ħω, equals the effective work function, ϕ_{eff}. In the zero temperature limit Eq. (5) reduces to Eq. (4).

$$\varepsilon_n = \sigma_x\sqrt{\frac{\hbar\omega-\phi_{eff}}{3mc^2}} \quad (4)$$

$$\varepsilon_n = \sigma_x\sqrt{\frac{kT}{mc^2}}\sqrt{\frac{Li_3\left[-Exp\left[\frac{e}{kT}\left(\hbar\omega-\phi_{eff}\right)\right]\right]}{Li_2\left[-Exp\left[\frac{e}{kT}\left(\hbar\omega-\phi_{eff}\right)\right]\right]}} \quad (5)$$

$$Li_n[z] = \frac{(-1)^{n-1}}{(n-2)!}\int_0^1 \frac{1}{t}Log[t]^{n-2}\,Log[1-zt]\,dt$$

*Work supported by US DOE contract DE-AC02-76SF00515.

#tvecchio@slac.stanford.edu

ISBN 978-3-95450-134-2

To derive Eq. (4) or (5) two physical models are used. The first is the Sommerfeld free electron model describing electronic states and their occupational probabilities. In this model electrons are bound by a uniform potential, they have a constant density of states and the occupational probability of these states is governed by Fermi-Dirac statistics. The second model used is the Spicer 3-step model identifying a sequence of steps involved in photoemission. In the first step electrons absorb photons gaining energy $\Delta E=\hbar\omega$ normal to surface. In the second step these electrons diffuse to surface. In the third step these electrons escape if they can, loosing energy $\Delta E=\phi_{eff}$ normal to surface.

In the Sommerfeld model all metallic surfaces are treated identically. Unfortunately this is not always reliable for predicting emittance. The reason for this is that the electronic structure of the material has not been accounted for. Figure 2 illustrates the importance of crystallographic grains in photocathodes. It is generally agreed that the electronic structure should be included to improve the accuracy of emission models.

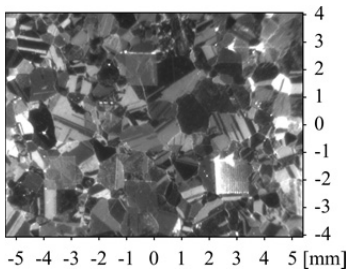

Figure 2: Optical image of a copper photocathode showing a large number of single crystal grains and illustrating the importance of crystallographic orientation.

METHODS

Electronic structure calculations have been incorporated into a photoemission model. The electronic structure calculations were performed using Density-Functional Theory (DFT), a widely accepted technique for calculating the ground state electronic structure of a material. The basis of DFT is an assumption that the exact N-body Schrödinger equation for a system of electrons

$$\left(-\frac{1}{2}\nabla^2+\frac{1}{2}\sum_{i\neq j}\frac{1}{|r_i-r_j|}-\sum_{i,I}\frac{Z_I}{|r_i-R_I|}+\frac{1}{2}\sum_{I\neq J}\frac{Z_I Z_J}{|R_I-R_J|}\right)\Psi\left(r_1,r_2,\rightleftharpoons\right)=E\Psi\left(r_1,r_2,\rightleftharpoons\right) \quad (6)$$

can be described by an equivalent set of N, 1-body Kohn-Sham equations.

$$\left(-\frac{1}{2}\nabla_i^2+\frac{1}{2}\int\frac{n(r')}{|r-r'|}dr'-\sum_I\int\frac{Z_I n(r')}{|r'-R_I|}dr'+\frac{1}{2}\sum_{I\neq J}\frac{Z_I Z_J}{|R_I-R_J|}+\varepsilon_{xc}\left[n(r)\right]\right)\psi_i(r)=\varepsilon_i\psi_i(r) \quad (7)$$

An "exchange-correlation" term is added ad-hoc to the Kohn-Sham equations and defined to be anything such that this equivalency is true. The approach was laid down in the 1960s [5, 6] and has been improved on since then.

ABINIT was used in these simulations. ABINIT is a freely distributed software package for DFT calculations. It emphasizes valence band phenomena by replacing the core electron charge density with norm-conserving pseudopotentials. This simplifies the problem, allowing for a decreased plane-wave basis set to be used in solving the Kohn-Sham equations. In these simulations Troullier-Martins type pseudopotentials were used.

ABINIT relies on periodic boundary conditions. As a result, surface electronic structure can be calculated using a slab supercell. Bulk calculations were done with a fixed lattice constant (3.615 Å) but the ionic positions in the slab calculations were allowed to relax. The final slab thicknesses were 42.1 Å for Cu(100), 30.4 Å for Cu(110) and 30.2 Å for Cu(111).

Additional simulation details are as follows. A local density approximation Teter-Pade parameterization was used for the exchange-correlation functional. The occupational probability of states was calculated using 0.01 Hartree "cold smearing". The energy cutoff was 30 Hartree for the slab calculations and 50 Hartree for the bulk calculations. In general the DFT convergence criterion was that of a difference in total energy of $1\text{x}10^{-6}$ Hartree twice in a row.

Once a set of eigenvectors and eigenvalues were calculated then they were expanded using symmetry operations to fill the Brillouin Zone. The number of eigenvectors used varied from a minimum of 16^2=256 for slab calculations to 50^3=125000 for bulk calculations. The discrete set of eigenvectors and eigenvalues were made continuous by linearly interpolating between them.

The physical model governing the emission aspects of the simulations was based on the Spicer model used to derive Eq. (4) and (5) with step 2 omitted. K-space was searched randomly until at least 10^3 states (or more) with sufficient energy and momentum for emission were found. These states were emitted and RMS values were calculated based on the resulting distribution.

ISBN 978-3-95450-134-2

RESULTS

The first results reported are simple demonstrations that the electronic structure of copper was calculated correctly. Figure 3 shows the Fermi surface from copper made by mapping the Fermi energy in K-space. The resulting shape is common to face-centered cubic metals.

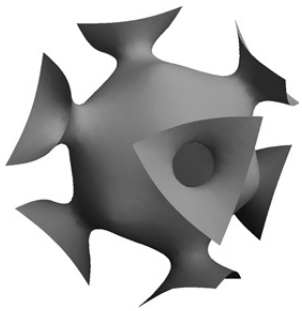

Figure 3: Fermi surface from copper. The shape of this surface is common and serves as a demonstration that the electronic structure was calculated correctly.

Figure 4 gives the simulated bulk density of states from copper. This result was also in line with expectations.

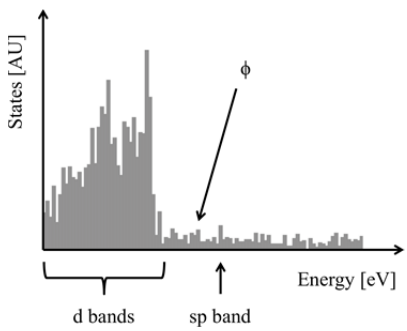

Figure 4: Bulk density of states for copper. The sp band in copper is separated from the d bands and is the reason that copper behaves like a free-electron metal.

Table 1: Surface Work Function Calculations using Supercell Slabs. The results of the current simulations are given in the first line of the table. The values are reasonably consistent with other published work.

Cu(111)	Cu(100)	Cu(110)		Source
5.02	4.88	4.65	calc	Vecchione, T.
5.02	4.64	4.52	calc	Schroder, A. *unpublished at present
5.31	5.02	4.81	calc	Fall, C.
5.19	4.95	4.9	calc	Rodach, T., Bohnen, K. P., & Ho, K. M.
5.2	4.94	4.68	calc	Li, W., & Li, D. Y.
4.94	4.59	4.48	exp	Gartland, P. O., Berge, S., & Slagsvold, B. J.
4.98	4.83	4.45	exp	Haas, G. A., & Thomas, R. E.
4.63	4.45	4.4	exp	Peralta, L., Margot, E., Berthier, Y., & Oudar, J.
5.54	5.15	4.92	exp	Delchar, T. A.

The supercell slab calculations produced values for work functions that were reasonably consistent with other published work. These results are summarized in Table 1.

The emission components of the simulations were verified by comparing the results with available angle-resolved photoemission spectroscopy (ARPES) data from copper. This comparison is shown in Figure 5.

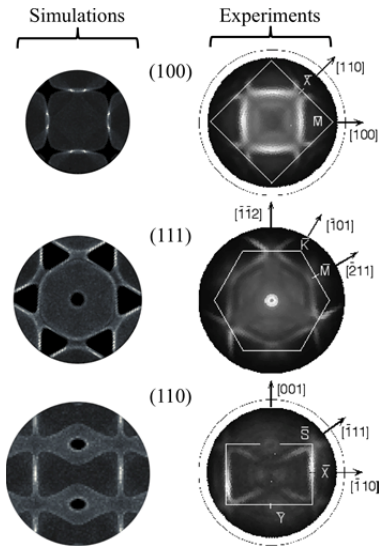

Figure 5: Verifying the emission model. The experimental data is reproduced from [7]. The excitation energy was $\hbar\omega$=21.2 eV (He) and in the simulations a bandwidth of ΔE = 0.1 eV was applied to the final result.

Having demonstrated that the simulations give reasonable results, the following are the results from copper, shown in Figures 6, 7 and 8.

Cu(100) and Cu(110) are well described by the Sommerfeld free electron model. Cu(110) has a much lower work function the Cu(100) but based on parameterized fits to the Dowell-Schmerge formula (Eq. (4) it also a much lower effective mass.

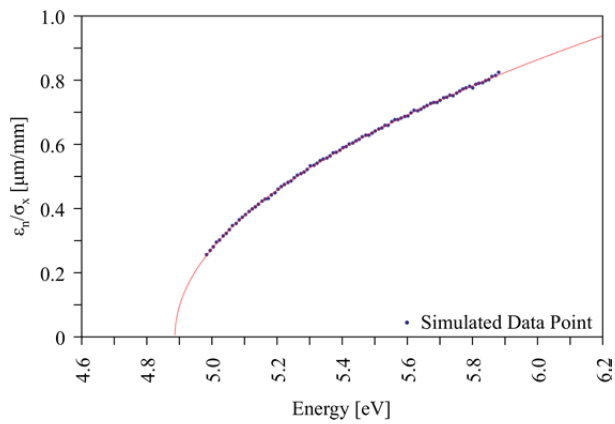

Figure 6: Emittance as a function of excitation energy for Cu(100). The slab calculation gives a work function of ϕ = 4.88 eV. Fitting the simulated data gives the same work function with an effective mass of m = 0.98 m_e.

ISBN 978-3-95450-134-2

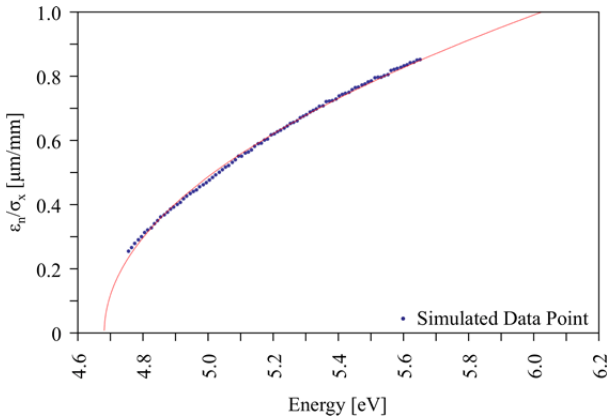

Figure 7: Emittance as a function of excitation energy for Cu(110). The slab calculation gives a work function of ϕ = 4.65 eV. Fitting the simulated emittance data gives a slightly different parameterization of m = 0.88 m_e and ϕ = 4.68 eV.

Cu(111) has a discontinuity in emission due a neck in the Fermi surface in this direction. Bulk Cu(111) would make a poor photocathode. However the gap in emission provides an interesting opportunity for a surface state to create a possibly lower emittance photocathode. This needs further study.

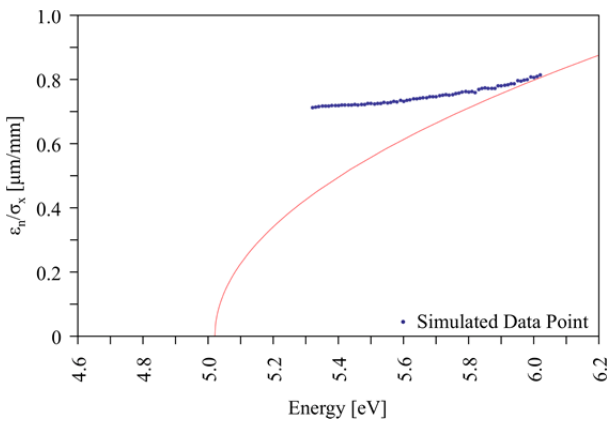

Figure 8: Emittance as a function of excitation energy for Cu(111). The slab calculation gives a work function of ϕ = 5.02 eV. The region where there is no emission comes from the neck in Fermi surface.

The effect of an applied electric field on the surface of a photocathode is to effectively lower the work function an amount given by Equation 8.

$$\Delta\phi = \sqrt{\frac{eF}{4\pi\varepsilon_0}} \tag{8}$$

This so called "Schottky effect" at 60 MV/m produces a 0.294 eV reduction in the work function. Figure 9 is a plot of emittance from Cu(100) and Cu(110) using Equation 4, the parameterized model fits from above and in the presence of a 60 MV/m extraction field.

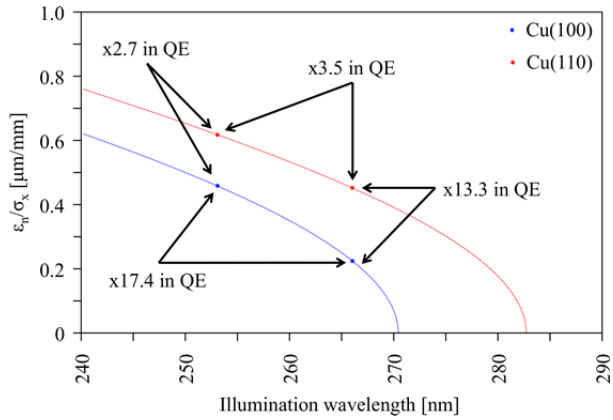

Figure 9: A comparison of emittance from Cu(100) and Cu(110) in the presence of a 60 MV/m extraction field. Factor differences in quantum efficiency are also listed to aid the comparison.

One finds that:
ε_n for Cu(100) at 253 nm = σ_x (0.46 μm/mm)
ε_n for Cu(110) at 253 nm = σ_x (0.62 μm/mm)
ε_n for Cu(100) at 266 nm = σ_x (0.22 μm/mm)
ε_n for Cu(110) at 266 nm = σ_x (0.45 μm/mm)

If quantum efficiency (QE) isn't a concern due to both an excess in overhead laser budget for a specific amount of charge and from being far from the damage threshold of the surface then minimal emittance would come from the Cu(100) surface illumined by 266 nm light. The projected value is actually a little below to the thermal limit of 0.23 μm/mm. This comes from having ignored Fermi statistics (temperature) in the model. The real value will be slightly higher than this but not so much so as to change the overall result. Under realistic operating conditions this is probably the best value that can be achieved.

CONCLUSIONS

In summary, the benefits to FELs from reducing photocathode emittance can be significant. Recognizing that experimental work is expensive, cost-effective numerical simulations have been performed. Within the model assumptions the Cu(100) surface was identified as having minimal emittance, particularly when illuminated by 266 nm light and extracted in a 60 MV/m gradient. These findings will guide future experimental work, leading to improved machine performance.

FUTURE PLANS

Several important physical phenomena have been left out of these simulations. In the near future it will be important to repeat these simulations including the effects of finite temperature occupational probabilities, the work function shift in the presence of surface oxide layers and having considered contributions from surface states.

ISBN 978-3-95450-134-2

In general the (111) surfaces of the face-centered cubic and the (100) surfaces of the body-centered cubic metals have exposed surface states. Figure 10 gives an example of one such case. This is important because surface states have well defined dispersion relations. The energy of a transition from an initial surface state ($\hbar\omega$) limits the transverse momentum allowed in the final state. If the final state is in vacuum, the result is anisotropic emission that is confined in both energy and momentum. It has been hypothesized that surface states could be a source for low emittance electron beams so the overall contribution of surface states needs to be considered.

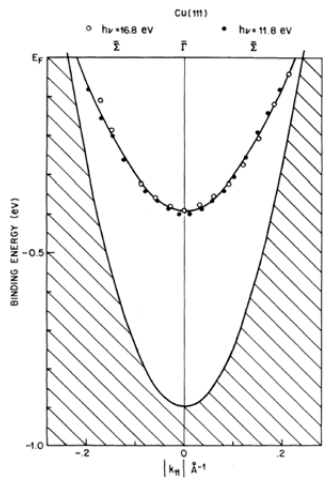

Figure 10: Image reproduced from [8] showing a clear dispersion relationship of the exposed Cu(111) surface state. The region where there is no emission from the bulk states comes from the neck in the Fermi surface.

The set of face-centered cubic and body-centered cubic metals shown in Figure 11 are expected to exhibit phenomenogically similar emission characteristics to those found in copper. In the future emittance simulations from these metals will be systematically parameterized to identify surfaces with large effective masses that could possibly produce low emittance beams. A group led by W. A. Schroeder has recently published results [9,10] showing good success with similar structure based comparative efforts.

									bcc	
									fcc	
Li	Be									
Na	Mg									
K	Ca	Sc	Ti	V	Cr	Mn	Fe	Co	Ni	Cu
Rb	Sr	Y	Zr	Nb	Mo	Tc	Ru	Rh	Pd	Ag
Cs	Ba		Hf	Ta	W	Re	Os	Ir	Pt	Au

Figure 11: The set of face-centered cubic and body-centered cubic metals for which the effective masses of low index surfaces will be calculated.

Simulations are a preliminary step to identifying photocathodes for use. Before this can happen the results of the simulations must be experimentally verified. For this a strategy such as the one illustrated in Figure 12 could be used to test single crystal photocathodes for the LCLS-I.

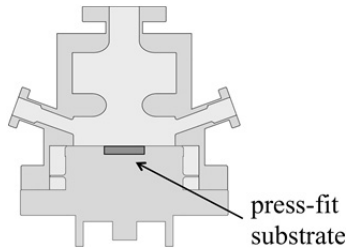

Figure 12: Experimental setup for testing single crystal photocathodes in a high gradient RF gun. This press-fit substrate strategy is similar to one that has been used at the UCLA/PEGASUS facility.

Finally the algorithm for calculating emittance from metallic photocathodes can be adapted to calculate emittance from semiconductor photocathodes. This will make the work relevant for future FELs such as the LCLS-II. The goal will be to search through appropriate semiconductors to find ones with large effective masses at their band gaps that could possibly produce low emittance beams.

ACKNOWLEDGMENT

The author would like to thank W. Andreas Schroeder at the University of Illinois at Chicago for all of his helpful suggestions.

REFERENCES

[1] M. Xie, "*Design optimization for an X-ray free electron laser driven by SLAC linac*", Proceedings of the 1995 Particle Accelerator Conference, May 1-5, 1995, Dallas, USA, 183-185.
[2] Z. Huang and K. J. Kim, *Phys. Rev. ST Accel. Beams* **10** 3, 034801 (2007).
[3] D. Dowell and J. Schmerge, *Phys. Rev. ST Accel. Beams* **12** 11, 074201 (2009).
[4] T. Vecchione et al, "*Quantum Efficiency and Transverse Momentum from Metals*", Proceedings of FEL'13, August 25-30, 2013, New York, USA, TUPSO83.
[5] P. Hohenberg and W. Kohn, *Phys. Rev.* **136**, B864 (1964).
[6] W. Kohn and L.J. Sham, *Phys. Rev.* **140**, A1133 (1965).
[7] P. Aebi et al., *Surf. Sci.* **307**, 917-921 (1994).
[8] S. D. Kevan, *Phys. Rev. Lett.* **50** 7, 526 (1983).
[9] T. Li, B. L. Rickman and W. A. Schroeder, *J. Appl. Phys.* **117** 13, 134901 (2015).
[10] T. Li, B. L. Rickman and W. A. Schroeder, *Phys. Rev. ST Accel. Beams* **18** 7, 073401 (2015).

ISBN 978-3-95450-134-2